

Elucidating the role of the hole-extracting electrode on the stability and efficiency of inverted $\text{CsSnI}_3 / \text{C}_{60}$ perovskite photovoltaics

K. P. Marshall¹, M. Walker², R. I. Walton¹, and R. A. Hatton^{1*}

¹Department of Chemistry, University of Warwick, Coventry, CV4 7AL, UK.

²Department of Physics, University of Warwick, Coventry, CV4 7AL, UK.

*Ross.Hatton@warwick.ac.uk

Supporting Information

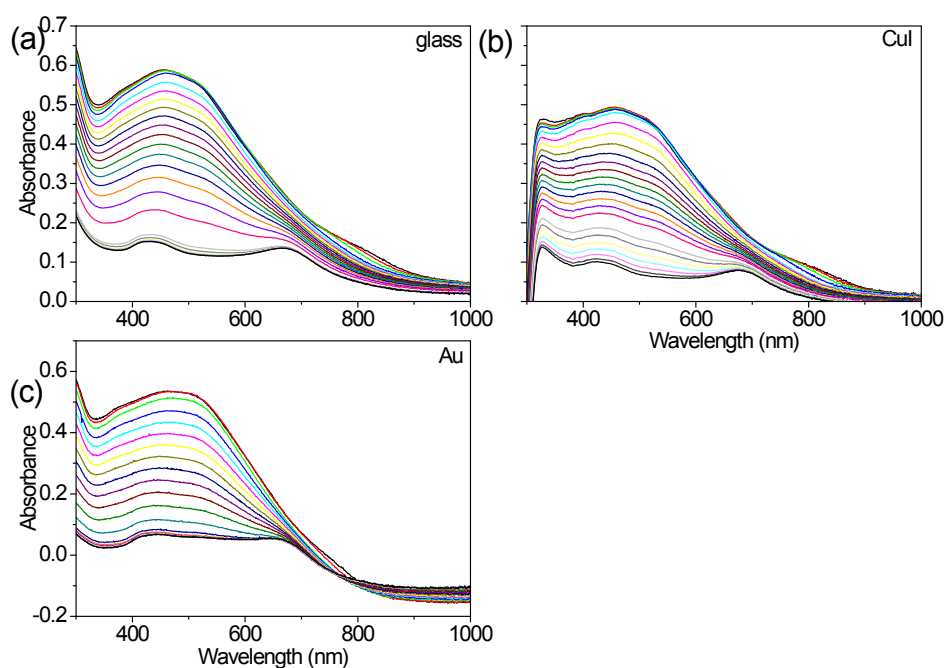


Figure S1: Evolution of electronic absorption spectrum of $\text{CsSnI}_3 + 10 \text{ mol\% SnCl}_2$ films deposited on glass **(a)**, ITO:CuI **(b)** and Au **(c)**. In all cases the CsSnI_3 solution was 8 wt% by total mass of solids which resulted in a film thickness of $\sim 50 \text{ nm}$. In each case the background has been subtracted.

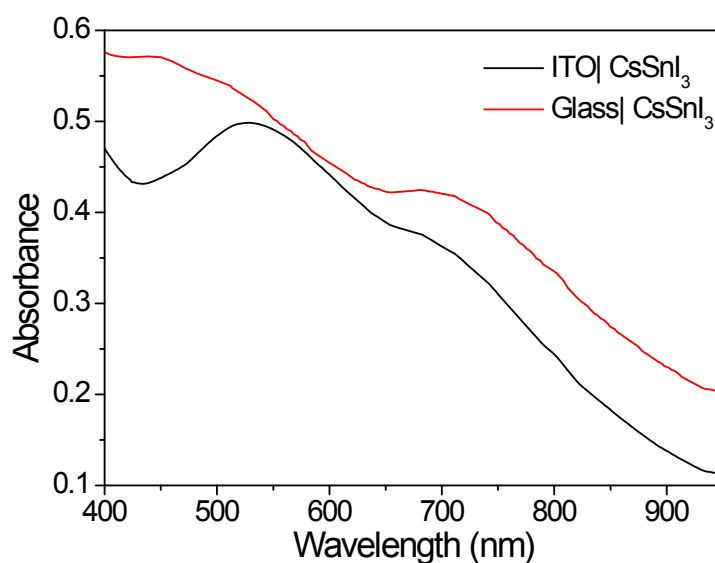


Figure S2: Optical simulation using the Essential Macleod (Thin Film Centre Inc.) simulation package, showing the difference in absorbance for a 50 nm CsSnI₃ film on glass and ITO coated glass assuming a ITO thickness of ~ 140 nm and CsSnI₃ film with an idealised uniform slab-like structure. These simulations show that optical interference due to the ITO layer gives rise to a local minimum in the absorption spectrum close to a wavelength of 400 nm, the exact position of which depends sensitively on the optical properties and thickness of the ITO layer.

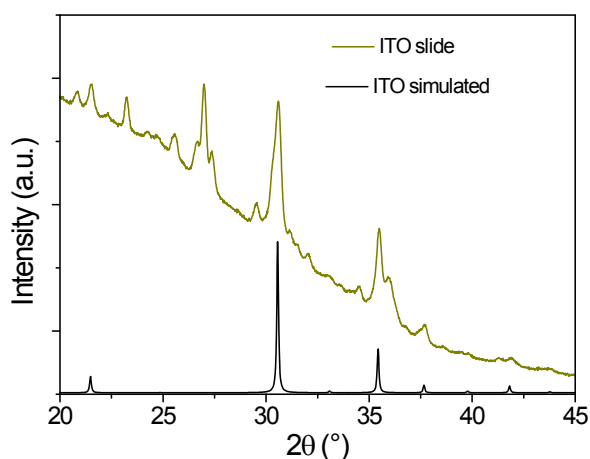


Figure S3: Measured XRD pattern of an ITO glass slide (green) and simulated XRD pattern for ITO (black).

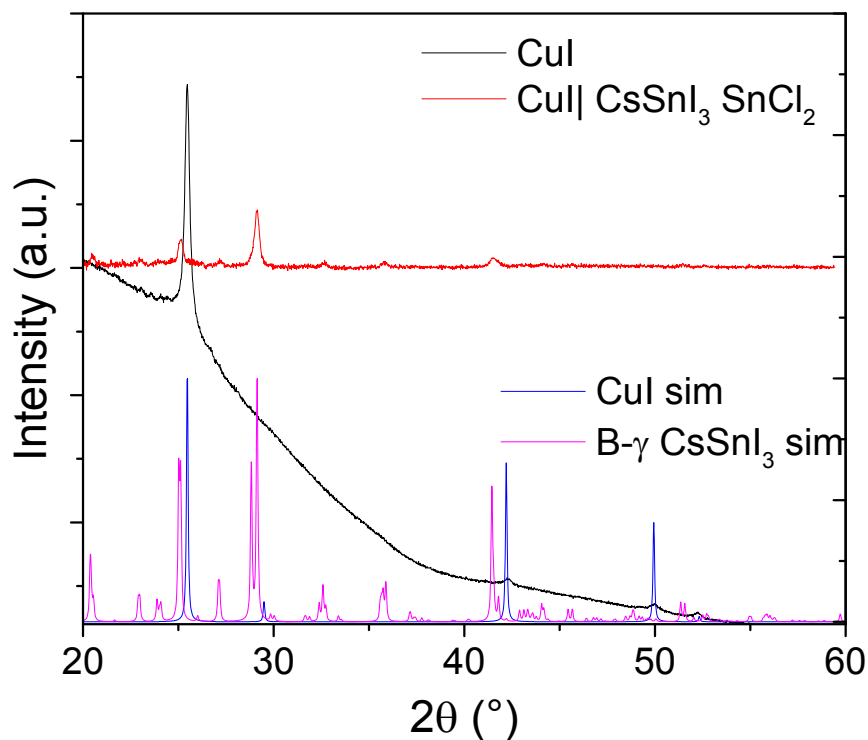


Figure S4: XRD pattern of CsSnI₃ on a glass | CuI (~40 nm) substrate, and a film of CuI on glass. Simulated patterns of CsSnI₃ and CuI also shown.

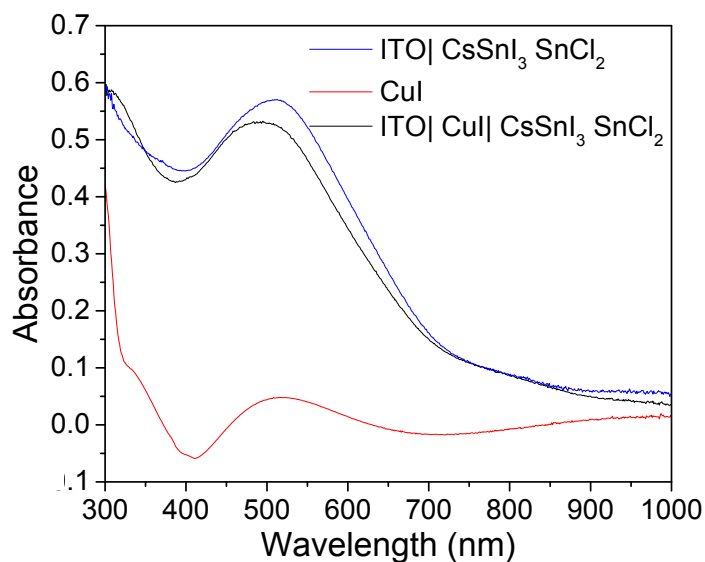


Figure S5: Electronic absorption spectra of a CsSnI₃:SnCl₂ (10 mol%) film supported on ITO glass (blue); a ~ 40 nm CuI film on ITO glass (red); a CsSnI₃:SnCl₂ film on CuI coated ITO glass (black). In all cases ITO glass was used as the background. The apparent negative absorbance in some parts of the CuI spectrum is attributed to the CuI film functioning as an anti-reflective layer over particular wavelength ranges.

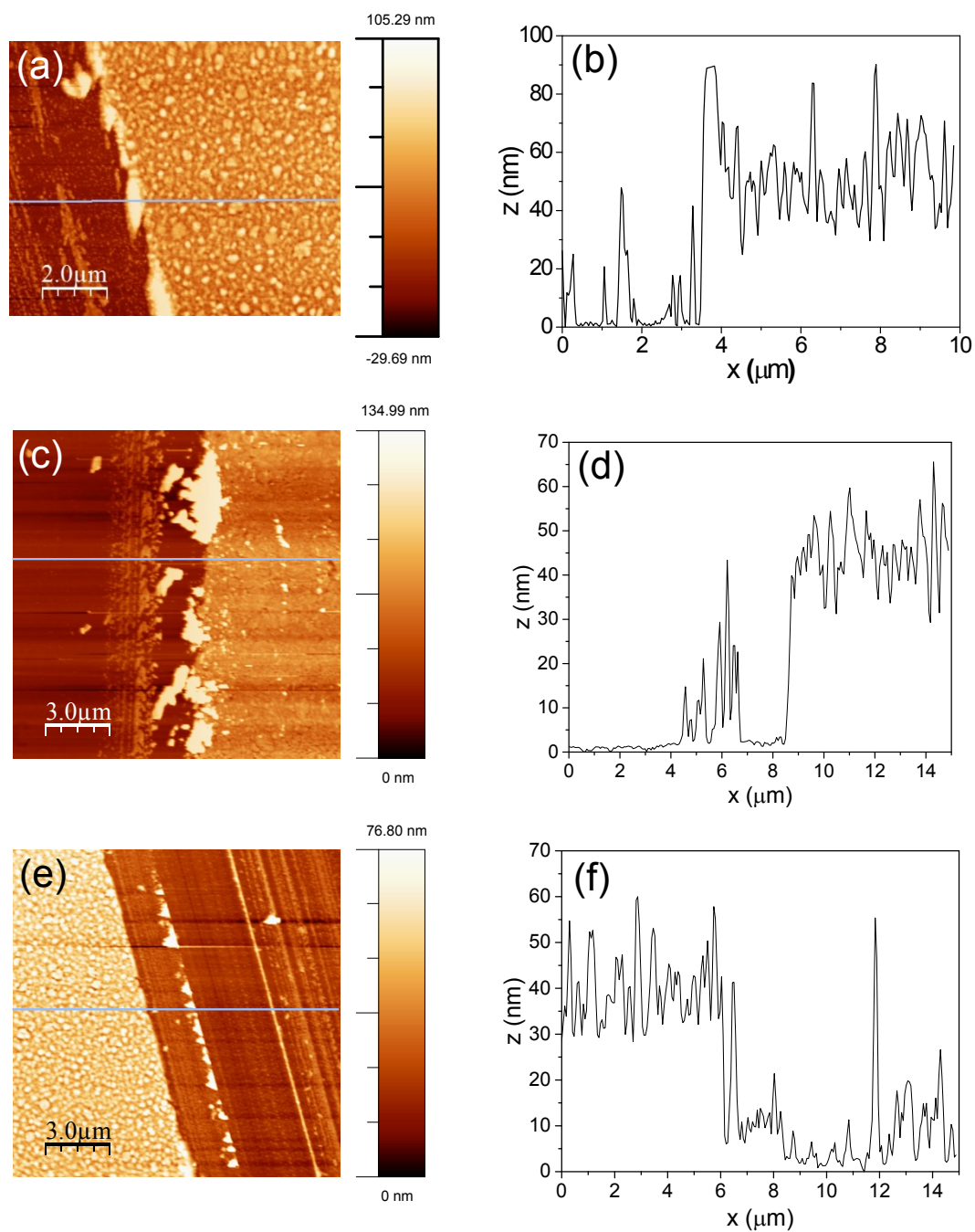


Figure S6: AFM image of surface topography **(a)** and cross-section **(b)** of a film of $\text{CsSnI}_3\text{:SnCl}_2$ deposited on glass.; AFM image of surface topography **(c)** and cross-section **(d)** of a film of CuI deposited on glass.; AFM image of surface topography **(e)** and cross-section **(f)** of a film of $\text{CsSnI}_3\text{:SnCl}_2$ deposited onto a film of CuI on glass.

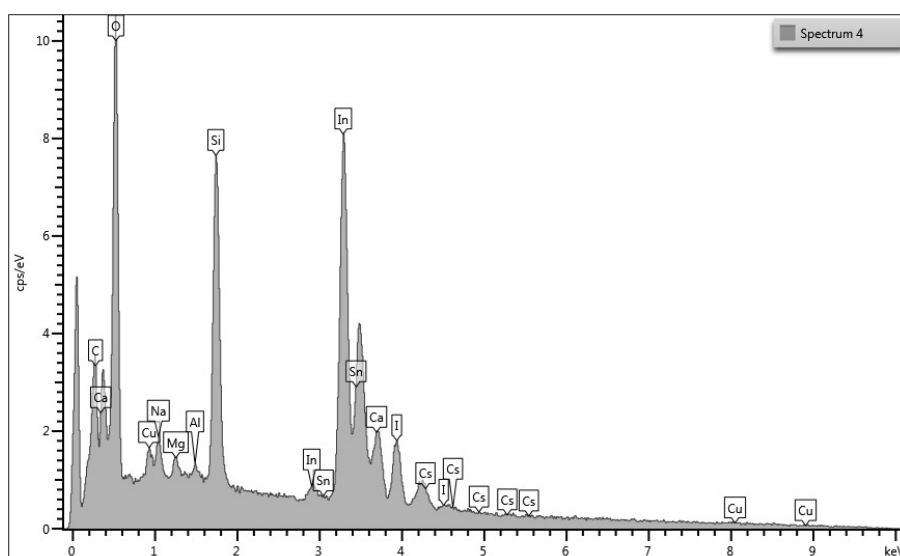


Figure S7: Energy-dispersive X-ray spectrum of a film of $\text{CsSnI}_3:\text{SnCl}_2$ deposited onto a ~40 nm thick CuI film supported on an ITO glass substrate.

Table S1: Average atomic composition of five EDX scans of a film of $\text{CsSnI}_3:\text{SnCl}_2$ onto a ~40 nm thick CuI film supported on an ITO glass substrate.

Element	Cs	Sn	I	Cl	In
Atom %	3.79	13.88	9.82	0.35	72.09

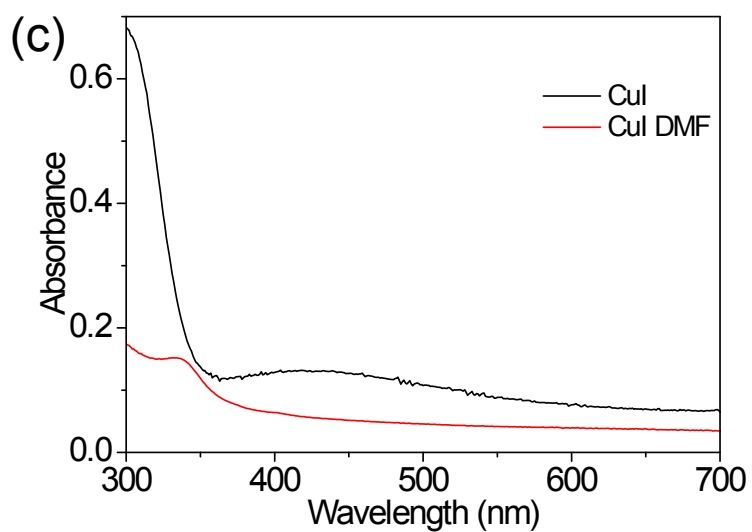
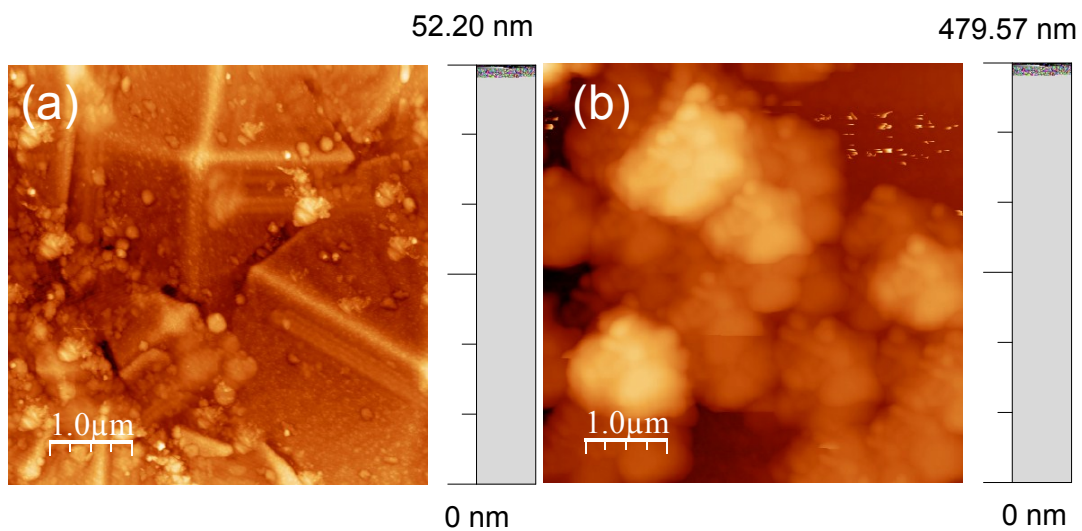


Figure S8: AFM images of CuI deposited on glass **(a)** before and **(b)** after spin-casting DMF on top of the film: **(c)** UV/ vis/ NIR spectra of films of CuI with (red) and without (black) DMF spin-casted on top.

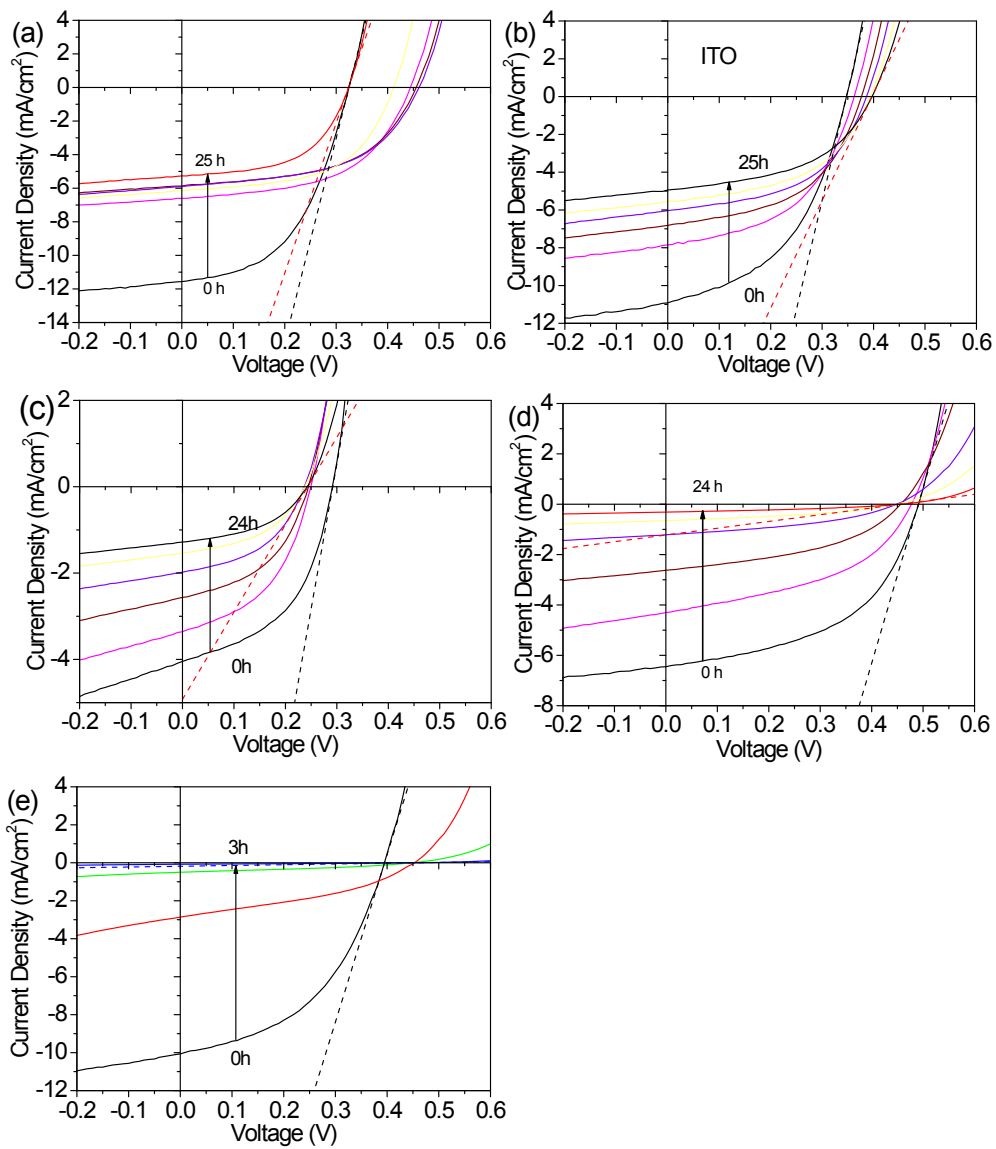


Figure S9: JV plots of PV devices with the structure: hole-extracting electrode | CsSnI₃:SnCl₂| C₆₀| BCP| Al where the hole-extracting electrode is ITO (**a**) (data in Figure 5a) and (**b**) (data in Figure 5b); Au (**c**); ITO| PEDOT:PSS (**d**); and ITO| CuI (**e**) substrates. Tangents of first and last scans at V_{oc} given as dotted lines.

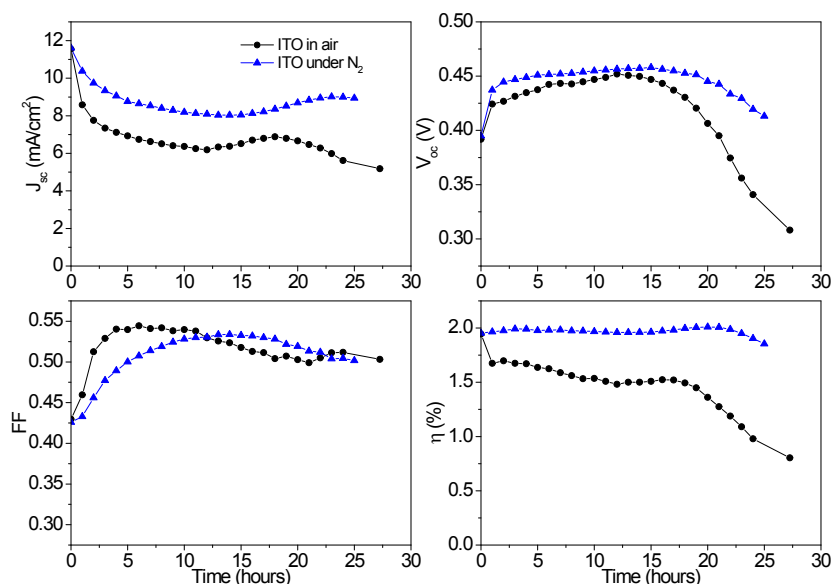


Figure S10: Representative performance of 6 mm² CsSnI₃:SnCl₂ PPV devices with the structure; ITO | CsSnI₃:SnCl₂ | C₆₀ | BCP | Al tested in ambient air (black) and in a nitrogen atmosphere (< 1 ppm O₂, < 1 ppm H₂O) (blue) under constant 1 sun simulated solar illumination. After 45 minutes the device temperature had stabilised at ~ 50°C.

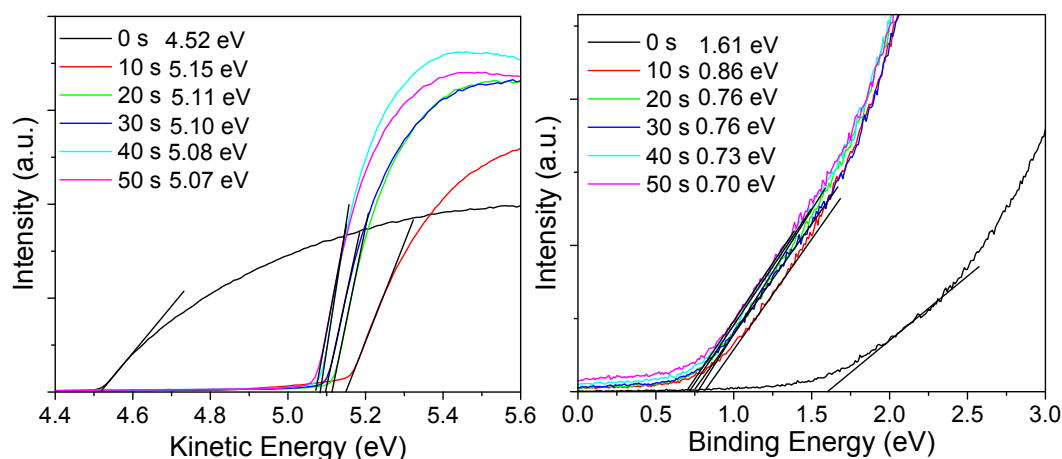


Figure S11: UPS spectrum of a film of Cs₂SnI₆ (supported on Au) formed by air oxidation of CsSnI₃. The secondary electron cut off region; left, and region near to the Fermi level, including the valance band edge; right. The sample was Ar⁺ ion etched for 0 to 50 s, in 10 sec steps to remove surface contaminants and adsorbed water. For t = 20, 30 and 40 seconds sputtering the data sets converge to the same value (within error) giving a valence band edge energy for Cs₂SnI₆ as 5.83 eV ± 0.05 eV below the vacuum level and work function of 5.1 eV. Literature values for the band gap of Cs₂SnI₆ range from 1.3 to 1.6 eV,¹⁻³ giving a value for the CB edge between 4.53 eV and 4.23 eV below the vacuum level.

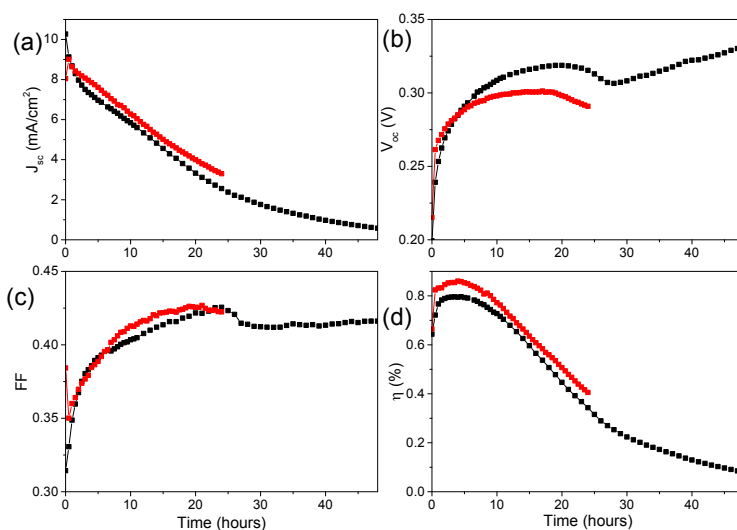


Figure S12: Current-voltage (J - V) characteristics of unencapsulated 74 mm² PPV devices with the structure; ITO glass / CsSnI₃ + 10 mol% SnCl₂ (8 wt%)/ C₆₀ / BCP / Al as a function of time under 1 sun constant illumination in air.

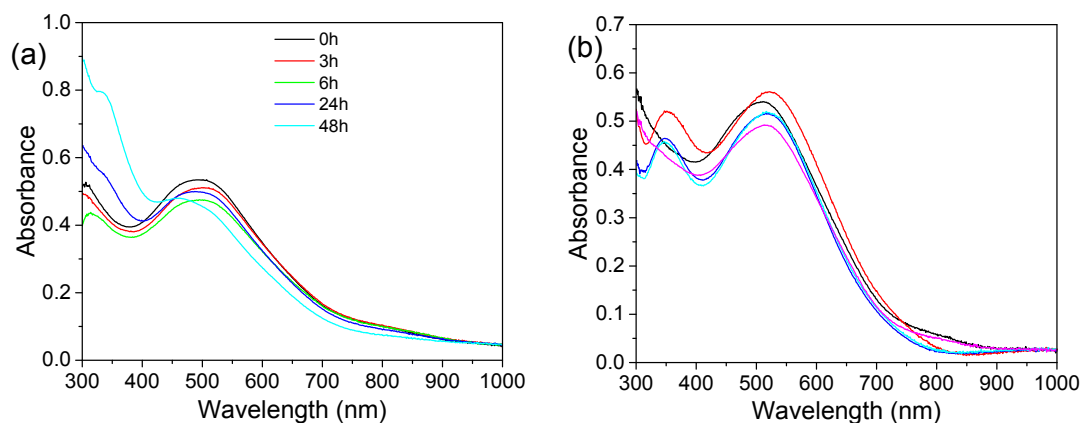


Figure S13: (a) Evolution of the electronic absorption spectrum of a ~ 50 nm CsSnI₃ film deconstructed from unencapsulated PV devices with the structure; ITO glass / CsSnI₃ + 10 mol% SnCl₂ (8 wt%)/ C₆₀ / BCP / Al after testing under 1 sun constant illumination in ambient air for 3, 6, 24 and 48 hours. After testing the devices were transferred to a nitrogen filled glovebox (< 1 ppm H₂O and O₂) where the top Al electrode was peeled off using carbon tape. It was then washed by immersing in anhydrous chlorobenzene three times to remove the SnCl₂ / C₆₀ / BCP layers before measuring the absorption spectrum. **(b)** Electronic absorption spectra of five CsSnI₃:SnCl₂ films on ITO glass prepared in the same way as used for devices in (a), demonstrating the variation in absorption across nominally identical films.

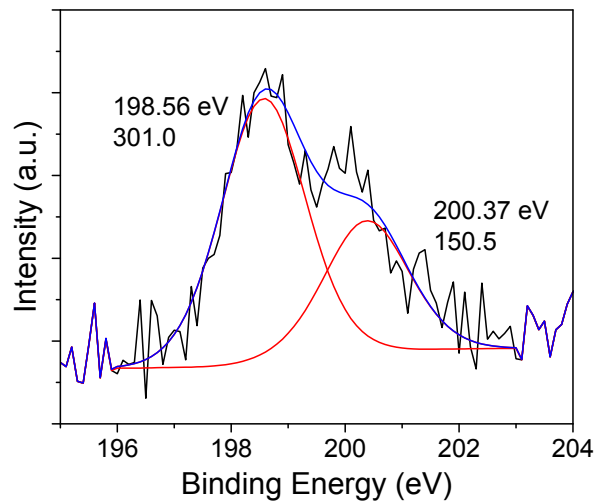
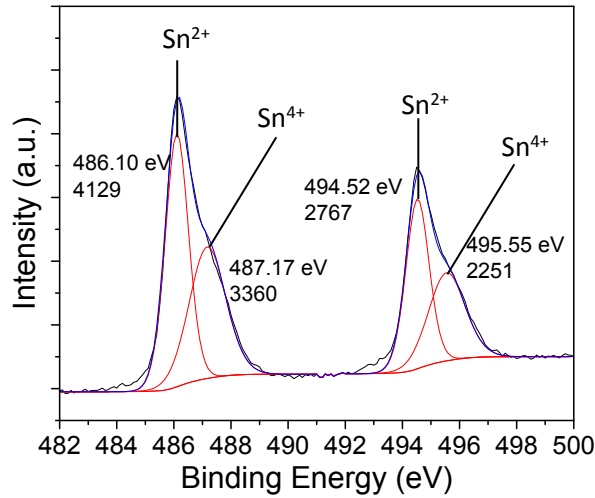


Figure S14: High resolution XPS spectrum of the Sn 3d region (upper) and Cl 2p region (lower) of the surface of a perovskite film recovered from a PV device with the structure: ITO glass / CsSnI₃ + 10 mol% SnCl₂ (8 wt%)/ C₆₀ / BCP / Al. The device was unencapsulated and was tested for 24 hours in ambient air under 1 sun continuous simulated solar illumination. After testing it was transferred to a nitrogen filled glovebox (< 1 ppm H₂O and O₂) and the top Al electrode was peeled off using carbon tape. It was then washed by immersing in anhydrous chlorobenzene three times to remove the SnCl₂ / C₆₀ / BCP layers before transferring to the vacuum chamber of the XPS spectrometer without exposure to ambient air. It is assumed that air ingress into the device results in the formation of a layer of Cs₂SnI₆ at the surface of the CsSnI₃ film that interfaces with the C₆₀ electron transport layer in the device. The Cs₂SnI₆ thickness was determined using the thickogram method⁴ based on the ratio of Sn 3d peak areas assigned to Sn²⁺ and Sn⁴⁺ oxidation states, which correspond to CsSnI₃ and Cs₂SnI₆ respectively^[5], and assuming an inelastic mean free path in Cs₂SnI₆ of 2.58 nm (estimated assuming a Cs₂SnI₆ density of 4.521 g/ cm³ using the method of S. Tanuma *et al.*^[6]).

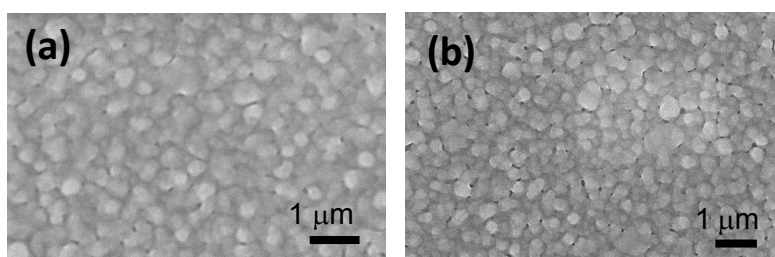


Figure S15: SEM images of (a) PC₆₁BM and (b) C₆₀ (40 nm), deposited on top of ITO|CsSnI₃ + 10% SnCl₂ substrates.

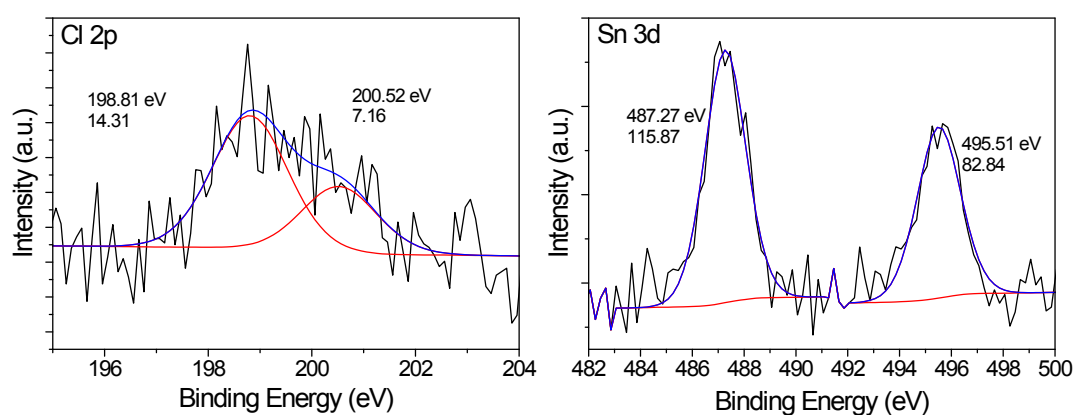


Figure S16: High resolution XPS spectra of the Cl 2p and Sn 3d regions at the point marked in the photograph (lower). The photograph shows the surface of device with the structure ITO|CsSnI₃:SnCl₂|C₆₀|BCP|Al, in which the BCP|Al and part of the C₆₀ layer has been removed using carbon tape to expose the interfacial region between the perovskite film and C₆₀.

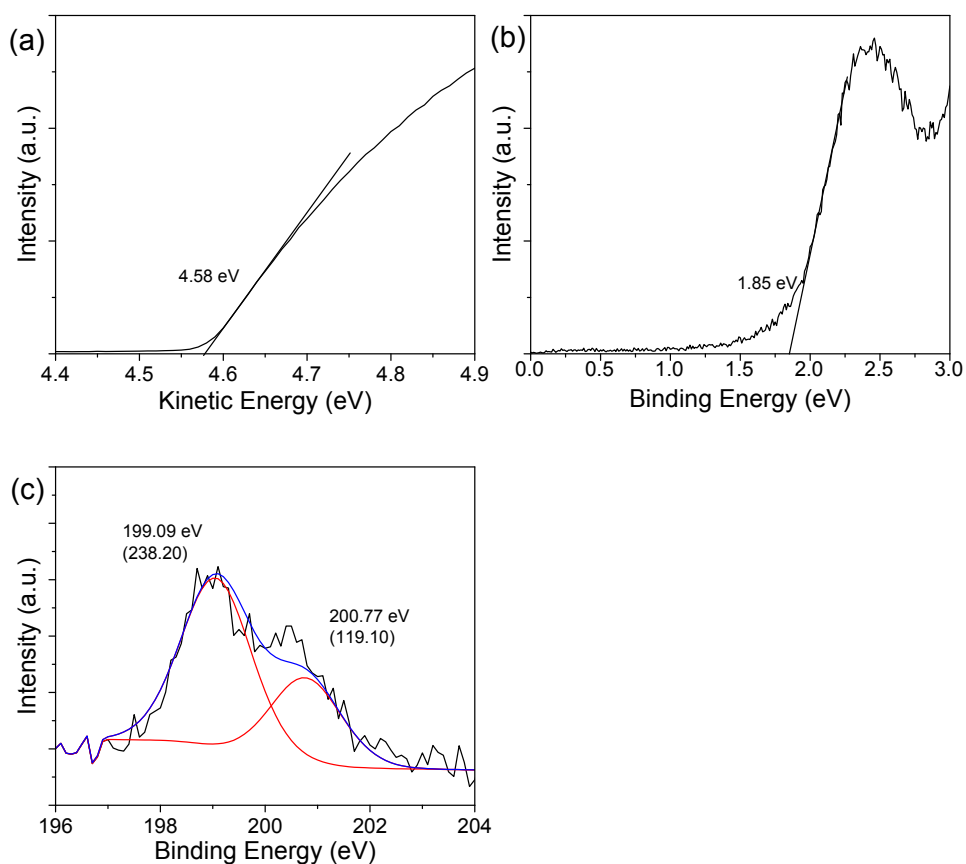


Figure S17: UPS spectrum of a film of C_{60} prepared from 5 mg/ml chlorobenzene solution with 0.5 mg/ml $SnCl_2$ showing (a) the secondary and (b) the primary cut-offs. (c) Cl 2p XPS spectrum of the same film.

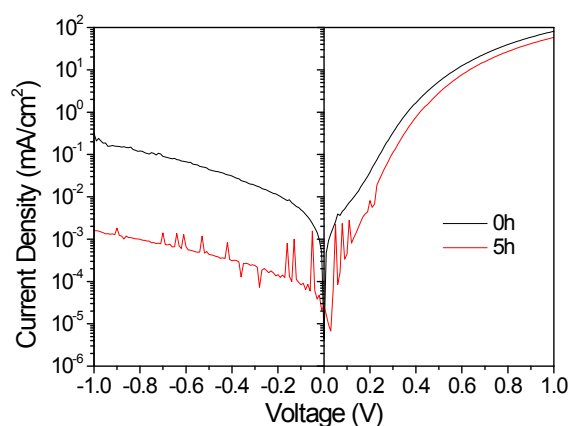


Figure S18: Representative log-linear dark current-voltage characteristic of the ITO| $CsSnI_3:SnCl_2$ | C_{60} |BCP|Al photovoltaic devices shown in Figure 5. These data show that the current in reverse bias is dramatically reduced after the device has been subjected to

constant 1 sun solar illumination for 5 hours, at which corresponds to the point at which the improvement in device fill-factor has saturated.

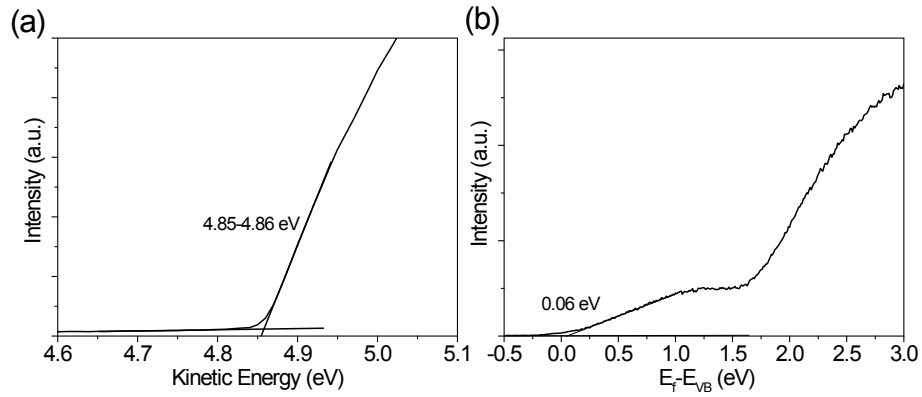


Figure S19: UPS spectrum (secondary electron cut-off **(a)** and valence band edge **(b)**) of CsSnI₃ on Au without exposure to the ambient environment.

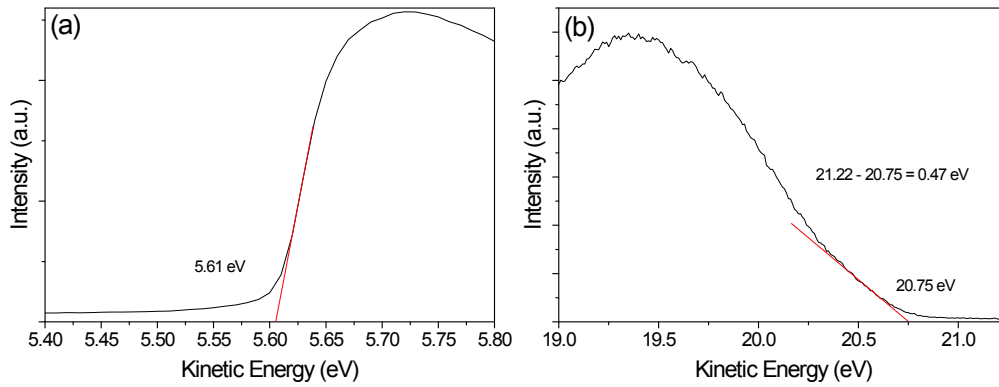


Figure S20: UPS spectrum (secondary electron cut-off **(a)** and valence band edge **(b)**) of CuI on ITO without exposure to the ambient environment.

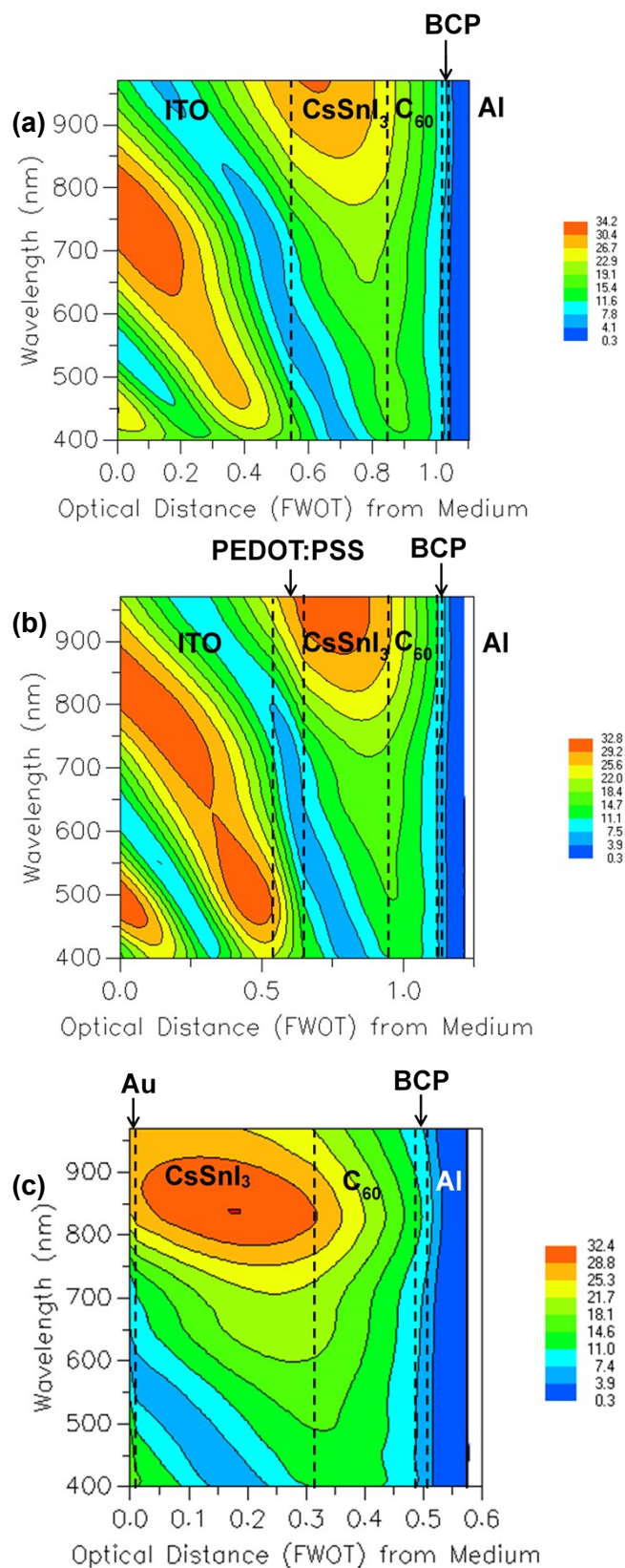


Figure S21: Electric component of optical field ($V\ m^{-1}$) in PV devices using ITO (a), ITO | PEDOT:PSS (b) and Au (c) as the hole-extracting electrode, modelled using the Essential Macleod, Thin Film Centre Inc. software simulation package.

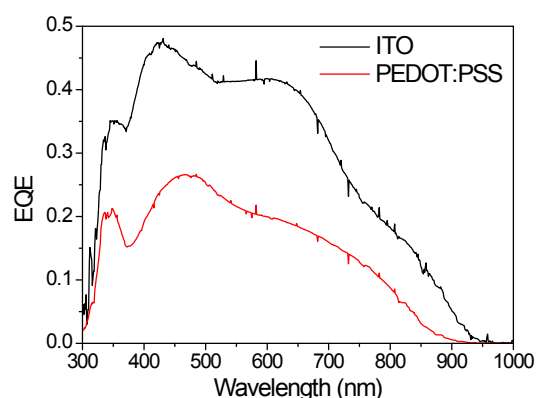


Figure S22: External Quantum Efficiency spectra of PV devices with the structure: ITO / CsSnI₃:SnCl₂ / C₆₀ / BCP / Al (black) and ITO | PEDOT:PSS | CsSnI₃:SnCl₂ / C₆₀ / BCP / Al (red).

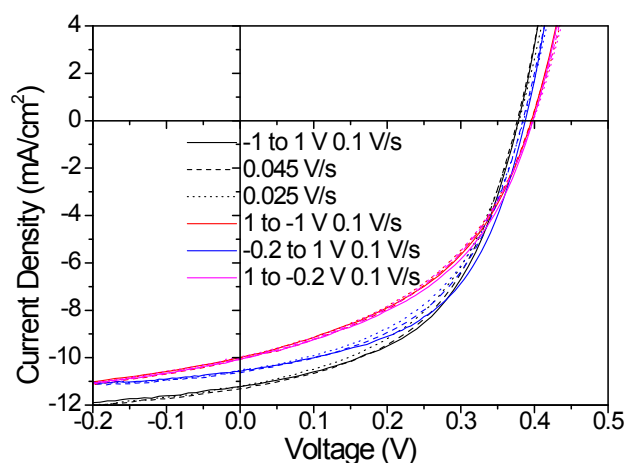


Figure S23: Current density - voltage plot of an ITO | CsSnI₃:SnCl₂ | C₆₀ | BCP | Al devices with different scan parameters.

- 1 B. Saparov, J.-P. Sun, W. Meng, Z. Xiao, H.-S. Duan, O. Gunawan, D. Shin, I. G. Hill, Y. Yan and D. B. Mitzi, *Chem. Mater.*, 2016, **28**, 2315–2322.
- 2 J. Zhang, C. Yu, L. Wang, Y. Li, Y. Ren and K. Shum, *Sci. Rep.*, 2014, **4**, 6954.
- 3 B. Lee, C. C. Stoumpos, N. Zhou, F. Hao, C. Malliakas, C. Yeh, T. J. Marks, M. G. Kanatzidis and R. P. H. Chang, *J. Am. Chem. Soc.*, 2014, **136**, 15379–15385.
- 4 S. Tanuma, C. J. Powell and D. R. Penn, *Surf. Interface Anal.*, 2003, **35**, 268–275.
- 5 K. P. Marshall, M. Walker, R. I. Walton, R. A. Hatton, *Nat. Energy* **2016**, *1*, 16178.
- 6 P. J. Cumpson and P. C. Zalm, *Surf. Interface Anal.*, 2000, **29**, 403–406.